Bioartificial Liver Support System Integrated with a DLM/GelMA-Based Bioengineered Whole Liver for Prevention of Hepatic Encephalopathy *via* Enhanced Ammonia Reduction

Guohua Wu[1, 2], Di Wu[1, 2], James Lo[3], Yimin Wang[1, 2], Jianguo Wu[1, 2], Siming Lu[1], Han Xu[4], Xin Zhao[5], Yong He[6], Jun Li[1], Utkan Demirci[7, 8], Shuqi Wang[1, 2*]

[1] *State Key Laboratory for Diagnosis and Treatment of Infectious Diseases, National Clinical Research Center for Infectious Diseases, Collaborative Innovation Center for Diagnosis and Treatment of Infectious Diseases, The First Affiliated Hospital, College of Medicine, Zhejiang University, Hangzhou, Zhejiang Province, 310003, China*

[2] *Institute for Translational Medicine, Zhejiang University, Hangzhou, Zhejiang Province, 310029, China*

[3] *Department of Bioengineering, University of California Berkeley, Berkeley, CA, 94720, USA*

[4] *Department of Building Environment and Energy Engineering, Xi'an Jiaotong University, Xian, Shanxi Province, 710049, China*

[5] *Department of Biomedical Engineering, The Hong Kong Polytechnic University, Hong Kong SAR, China*

[6] *State Key Laboratory of Fluid Power and Mechatronic Systems, Key Laboratory of 3D Printing Process and Equipment of Zhejiang Province College of Mechanical Engineering, Zhejiang University, Hangzhou, Zhejiang Province, 310029, China*

[7] *Bio-Acoustic MEMS in Medicine (BAMM) Laboratory, Canary Center at Stanford for Cancer Early Detection, Department of Radiology, Stanford University, School of Medicine, Palo Alto, CA 94304, USA*

[8] *Department of Electrical Engineering (By courtesy), Stanford University, Stanford, CA 94305, USA*

*****Corresponding author: Shuqi Wang. E-mail: shuqi@zju.edu.cn

The following publication Wu, G., Wu, D., Lo, J., Wang, Y., Wu, J., Lu, S., ... & Wang, S. (2020). A bioartificial liver support system integrated with a DLM/GelMA-based bioengineered whole liver for prevention of hepatic encephalopathy via enhanced ammonia reduction. Biomaterials science, 8(10), 2814-2824 is available at https://doi.org/10.1039/c9bm01879d

Abstract

Although bioartificial liver support system (BLSS) plays an essential role in maintaining partial liver functions and detoxification for liver failure patients, hepatocytes are unanimously seeded in biomaterials, which lack the hierarchal structures and mechanical cues of native liver tissues. To address this challenge, we developed a new BLSS by combining a decellularized liver matrix (DLM)/GelMA-based bioengineered whole liver and a perfusion-based, oxygenated bioreactor. The novel bioengineered whole liver was fabricated by integrating photocrosslinkable gelatin (GelMA) and hepatocytes into a DLM. The combination of GelMA and DLM not only provided a biomimetic extracellular microenvironment (ECM) for enhanced cell immobilization and growth with elevated hepatic functions (*e.g.,* albumin secretion and CYP activities), but also presented biomechanical support to maintain the native structure of the liver. In addition, the perfusion-based, oxygenated bioreactor helped deliver oxygen to the interior tissues of the bioengineered liver, which was of importance for long-term culture. Most importantly, this new bioengineered whole liver decreased ammonia concentration by 45%, whereas direct seeding of hepatocytes in the naked DLM showed no significant reduction. Thus, the developed BLSS integrated with the DLM/GelMA-Based bioengineered whole liver can potentially help elevate liver functions and prevent HE in liver failure patients while waiting for liver transplantation.

Keywords: Decellularized liver matrix (DLM), Bioengineered whole liver, Bioreactor, GelMA, Ammonia, Hepatic encephalopathy (HE)

Introduction

According to the World Health Organization's estimates, more than 650 million people suffer from liver diseases worldwide, and 15% of them eventually develop liver failure[1]. Although liver transplantation is the most effective way of saving patients' lives, less than 10% of liver failure patients have access to donor livers[1]. Without liver transplantation, liver failure patients may develop severe symptoms such as HE, which leads to an over 50% mortality rate of liver-failure patients in the first year alone[1, 2]. As reported, more than 7,500 patients die from liver failure each year while waiting for suitable donor organs in the United States[3, 4]. To provide *in vitro* support, artificial liver support systems (ALSS) have been developed to remove toxins and relieve symptoms through hemodialysis or hemofiltration[5, 6]. Furthermore, BLSS has been developed by incorporating hepatocytes into ALSS to enable synthetic functions and biotransformation activities[7-9]. However, the effect of these measures for reducing the mortality of acute liver failure and acute-on-chronic liver failure is still limited[10].

In the current design of BLSS, hepatocytes are simply incorporated into biomaterials and cultured to provide partial hepatic functions, which, however, overlooks the importance of the extracellular microenvironment (ECM) in supporting cell growth and maintaining cell functions. It has been systemically reviewed that scaffolds[11], biological factors[12], and biomechanical cues[13] synergistically play a vital role in supporting growth hepatocyte growth, promoting cell-cell interactions, and enhancing the biosynthesis of albumin, urea, and cytochrome enzymes[14]. Although hydrogels[15, 16] and electrospun nanofibers[17, 18] can offer a viable 3D cell culture environment for hepatocytes, the lack of essential collagens and growth factors may undermine hepatic functions to a certain extent. Recently, key components derived from DLM (*e.g.,* major collagens and growth factors) have been utilized in supporting hepatocytes[19], showing enhanced ALB secretion and CYP activities[9, 20, 21]. However, the lack of histological structures of native tissues are still lacking for providing a biomimetic ECM similar to where hepatocytes reside *in vivo*. Thus, the essential components contributing to ECM should be considered to fully exploit hepatocytes in BLSS to supporting liver failure patients.

In this study, we developed a new type of BLSS by combining a bioengineered whole

liver and a perfusion-based, oxygenated bioreactor (Figure 1). The novel bioengineered whole liver was fabricated by integrating GelMA with hepatocytes into a DLM (Figure 1). Although DLM has been used to construct a bioengineered liver for liver transplantation[9, 22, 23], its function in BLSS has not been explored. Furthermore, the combination of GelMA and DLM not only provided a biomimetic ECM for enhanced cell immobilization and growth with elevated hepatic functions (*e.g.,* albumin secretion and CYP activities), but also presented biomechanical support to maintain the native space configuration of the liver. Most importantly, this new bioengineered whole liver reduced the initial concentration of ammonia from 5.66 mmol L^{-1} to 3.11 mmol L^{-1}, whereas direct seeding of hepatocytes in the naked DLM showed no significant reduction. Clearly, our results demonstrated that the DLM/GelMA-based bioengineered whole liver maintained long-term hepatic functions and enhanced ammonia reduction, which can potentially be integrated into BLSS to prevent HE in liver failure patients while waiting for suitable liver donors.

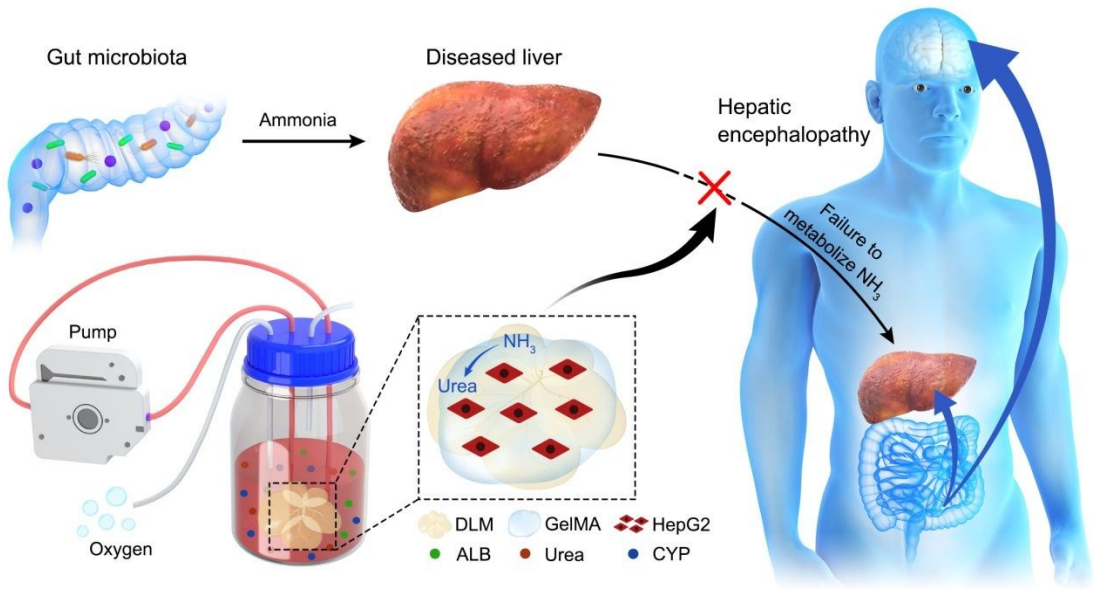

Figure 1. Schematic of the new BLSS integrated with a DLM/GelMA-based bioengineered whole liver for potential prevention of HE. In liver failure patients, hepatocytes cannot biotransform ammonia from the intestine, and excessive ammonia passes through the blood-brain barrier and enters the brain, which can cause HE. A bioengineered whole liver was fabricated by incorporating GelMA and HepG2 cells into DLM and continuously cultured in a perfusion-based oxygenated bioreactor. The DLM/GelMA-based bioengineered whole liver exhibits significantly enhanced biosynthesis and biotransformation capabilities, which has great potential to support

liver failure patients and to prevent the progression to HE.

Materials and methods

Liver excision

The livers were excised from Sprague-Dawley rats weighing 250-300 g according to the animal protocol (ZJU20170787) as approved by the Zhejiang University Experimental Animal Welfare Ethics Committee. After anesthetizing *via* intra peritoneal injection of 50 mg kg^{-1} pentobarbital sodium, the rats' abdomens were cut open to visualize the livers. A cannula was first inserted into the portal vein for subsequent perfusion. The vena cava and the remaining appendages were then dissected. The harvested livers were finally frozen overnight at -80 °C prior to decellularization.

Decellularization of the liver and characterization of DLM

To start the decellularization process, frozen livers were left to completely thaw at room temperature. A peristaltic pump (Longer Pump, Baoding, China) was then attached to the cannula, which was previously inserted in the portal vein, to allow sequential perfusion of a number of solutions for liver decellularization. First, phosphate buffer saline (PBS) was perfused for 1 hour. Second, 0.1% (w/v) sodium dodecyl sulfate (SDS) was perfused for 5 hours. Third, 1% (w/v) Triton X-100 was perfused for 30 minutes. The flow rate was set to 20 mL min^{-1}. To remove the residual nucleic acid completely, 80 U mL^{-1} Deoxyribonuclease I (DNase I) and 5 U mL^{-1} Ribonuclease (RNase) (Sigma-Aldrich, St. Louis, US) were perfused for an additional 30 minutes. Finally, the resultant DLM scaffold was rinsed with PBS containing 2% penicillin-streptomycin and amphotericin B (2.5 μg mL^{-1}) (Sangon Biotech, Shanghai, China). The DLM was transferred to a sterile Petri dish and stored at 4 °C prior to use.

Characterization of DLM was evaluated using scanning electron microscopy (SEM), HE staining and immunostaining. The microstructure of both DLM and native liver were dried, gold coated, and observed using SEM (Hitachi, Tokyo, Japan). HE staining was used to image cells and collagen fibers after decellularization. For immunostaining, native and decellularized livers were fixed in 4% formalin buffer, dehydrated, and finally embedded into paraffin. The resultant DLM was then sliced

and incubated with primary polyclonal antibodies from rabbit against collagen type I, collagen IV, fibronectin, or laminin (Abcam, Cambridge, UK). The sliced DLM scaffolds were then incubated with fluorescent secondary antibodies, which were goat anti-rabbit AlexaFluor® 594 (Abcam, Cambridge, UK). For identification of remaining cells within the DLM scaffolds, the sliced samples were stained with 4', 6-diamidino-2-phenylindole dihydrochloride (DAPI) (Sigma-Aldrich, St. Louis, US). All samples were imaged at a corresponding wavelength under a fluorescence microscope (Zeiss, Oberkochen, Germany).

Cell culture

For reseeding the DLM, the culture of HepG2 cells was expanded in a 75 cm^2 cell culture flask containing Dulbecco's modified Eagle's medium (DMEM) (Gibco, Melbourne, Australia), which was supplemented with 10% (v/v) of fetal bovine serum (FBS) (Gibco, Melbourne, Australia) and 1% (v/v) of penicillin/streptomycin (Sangon Biotech, Shanghai, China). The culture was carried out in an incubator with 5% CO_2 at 37 °C, and sub-culture was performed every three days.

Recellularization and culturing of the bioengineered whole liver

To prepare 5% (w/v) GelMA solution, 0.5g of GelMA (Suzhou Intelligent Manufacturing Research Institute, Suzhou, China) was added to 10 mL of DMEM medium with thorough mixing. HepG2 cells were first resuspended in 2 mL of DMEM at a final concentration of 1.0×10^7 cells mL^{-1}. The cell suspension was then centrifuged at 1,000 rpm for 3 minutes. The supernatant was discarded and replaced with 2 mL of 5% (w/v) GelMA. HepG2 cells were resuspended by pipetting up and down 5 times and then injected into the DLM using a 1 mL syringe. Once injected, GelMA was immediately exposed to ultraviolet (UV) light at a wavelength of 365 nm for 7 seconds for solidification. As a control, the same concentrations and volumes of HepG2 cells suspension were directly seeded in the naked DLM. These two types of bioengineered whole livers were then cultured in a 100 mL bioreactor containing 30 mL of DMEM. The medium was flowed *via* a peristaltic pump at a rate of 3 mL min^{-1}. The two types of bioengineered whole liver were cultured at 37°C with a mixed gas supply (95% O_2 and 5% CO_2) for 14 days. The culture supernatant was collected periodically for biological function analysis. 30 mL of DMEM medium was recirculated in the perfusion system and refreshed every 24 h.

Calculation of oxygen in the DLM/GelMA-based bioengineered whole liver

To understand the oxygen supply in the interior of the DLM/GelMA-based bioengineered whole liver, we calculated the oxygen concentration using the following equation:

$$C_r = \alpha P - \frac{1SN}{2\ D}(R_0{}^2 - X^2)$$

Cr represents the oxygen concentration in different parts of the bioengineered whole liver; the solubility coefficient for oxygen (α) at 37 °C in the medium was 2.08×10^{-3} mol m^{-3} $mmHg^{-1}$, the oxygen partial pressure of medium (P) was 90 mmHg [24]; the oxygen consumption rate (S) of HepG2 cells was 2.4×10^{-17} mol s^{-1} $cell^{-1}$ [25]; the cell density (N) was 1.07×10^{13} cells m^{-3}; the diffusion coefficient (D) of oxygen in gel was 2×10^{-9} m^2 s^{-1} [26]; the half thickness of organ (R_0) was about 1.5 mm, and X was the distance from surface to the center.

Detection of cell hypoxia

To evaluate the presence of hypoxia in cells in the bioengineered whole liver, the original medium in the culture flask was removed and replaced with fresh growth medium containing Image-iTTM green hypoxia reagent (Thermo Fisher Scientific, MA, USA) at a final concentration of 5 μM on day 14. The device was incubated at 37°C, 95% O_2 for 4 h before the bioengineered whole liver was washed twice with PBS, and the stained cells were observed under a confocal fluorescence microscope (A1, Nikon, Tokyo, Japan).

Characterization of HepG2 cells within the bioengineered whole liver

The viability of HepG2 cells within both the DLM/GelMA and the naked DLM based bioengineered whole liver was analyzed using a calcein-AM/propidium iodide kit (Live/Dead staining) (Dojindo, Kumamoto, Japan) on days 1, 3, 7, and 14. A dye solution, which allowed differentiation of live cells and dead cells, was prepared by adding 3 μL of calcein-AM and 2 μL of propidium iodide (PI) to 1 mL of PBS. Both types of bioengineered whole liver were stained by adding 10 mL of the calcein-AM/PI solution and then incubated for 2 hours at 37 °C, 95% O_2, and 5% CO_2 in the dark. The stained cells were analyzed using a confocal fluorescence microscope, and the obtained images were evaluated using Image J (National

Institutes of Health, Bethesda, MD, USA) software to quantify the cell viability and the cell growth rate in the same field-of-view.

Quantification of albumin and urea

The capacity to synthesize albumin (ALB) and urea by seeded HepG2 cells was assessed using a Rat Albumin ELISA Kit (ColorfulGene Biological Technology, Wuhan, China) and a Urea Assay Kit (Huding Biotechnology, Shanghai, China). The cell supernatant was collected on days 1, 3, 7, and 14 over a 14-day culture period. Both assays were carried out according to the manufacturers' respective protocols and the observance was measured using a multifunctional microplate reader (SpectraMax M5, Molecular Devices, San Jose, US). The concentration of ALB and urea was calculated according to their respective standard curves.

Toxic effects of NH_4Cl on HepG2 cells

To determine the toxic effects of ammonia on HepG2 cells, 100 µL of HepG2 cells (10^5 mL^{-1}) was seeded in a 96-well plate and cultured for 24 h with a mixed gas supply (95% O_2, and 5% CO_2) at 37°C. The seeded cells were then treated with 0, 5, 10, 30, 60 and 120 mM of NH_4Cl (Sangon Biotech, Shanghai, China), and each treatment was repeated in 3 microwells. Cell viability was assessed at 24 hours using Cell Counting Kit-8 reagent (MedChem Express, Monmouth Junction, NJ, USA). Briefly, 10 µL of CCK-8 solution was added to each microwell, and then the absorbance was evaluated at 450 nm after 2 hours.

Quantification of ammonia biotransformation

Both types of bioengineered whole liver were first cultured in DMEM with a perfusion rate of 3 mL min^{-1} for 12 hours. Then, the culture media was replaced with DMEM supplemented with 10 mM of NH_4Cl. Both types of bioengineered whole liver were cultured for another 48 hours, and the supernatant was collected. The concentration of ammonia in the culture supernatant was colorimetrically measured using a Urea Assay Kit (Huding Biotechnology, Shanghai, China) as also described in section 2.9.

Statistical analysis

Quantification data were expressed as average ± SD. A one-way analysis of variance

(ANOVA) was implemented to analyze the inter-group comparison *via* SPSS 19 (IBM Corporation, USA) software. Three independent trials were carried out unless otherwise stated. A statistical difference was determined when p was smaller than 0.05. The software package of GraphPad Prism 5 (GraphPad Software Inc., San Diego, CA, USA) was used for data analysis.

Results

Characterization of DLM

In this experiment, chemical solvents combined with physical destruction were used to prepare the DLM. First, liver cells were destroyed by repeated freezing and thawing, and then the livers were continuously perfused through the portal vein using SDS/Triton X-100. As with we previously reported, this protocol successfully produced decellularized livers[20, 27]. As shown in Figure 2A, prior to perfusion, the liver appeared dark red; after 9 hours of perfusion at a flow rate of 20 mL min^{-1}, the whole liver became colorless and transparent with clear choroidal structures. SEM results showed that the liver tissue after decellularization was loose and fibrous with a mesh structure (Figure 2B). H&E staining showed no clear nuclear and cytoplasmic components in the decellularized liver rather than in the pink extracellular matrix (Figure 2C). Immunohistochemical (IHC) staining showed that collagen I, collagen IV, fibronectin, and laminin were observed in the natural liver (Figure 2D). Following decellularization, all four aforementioned major ECM components were well preserved. DAPI staining was also conducted and a lack of blue staining of the nuclei of cells confirmed the success of decellularization (Figure 2E).

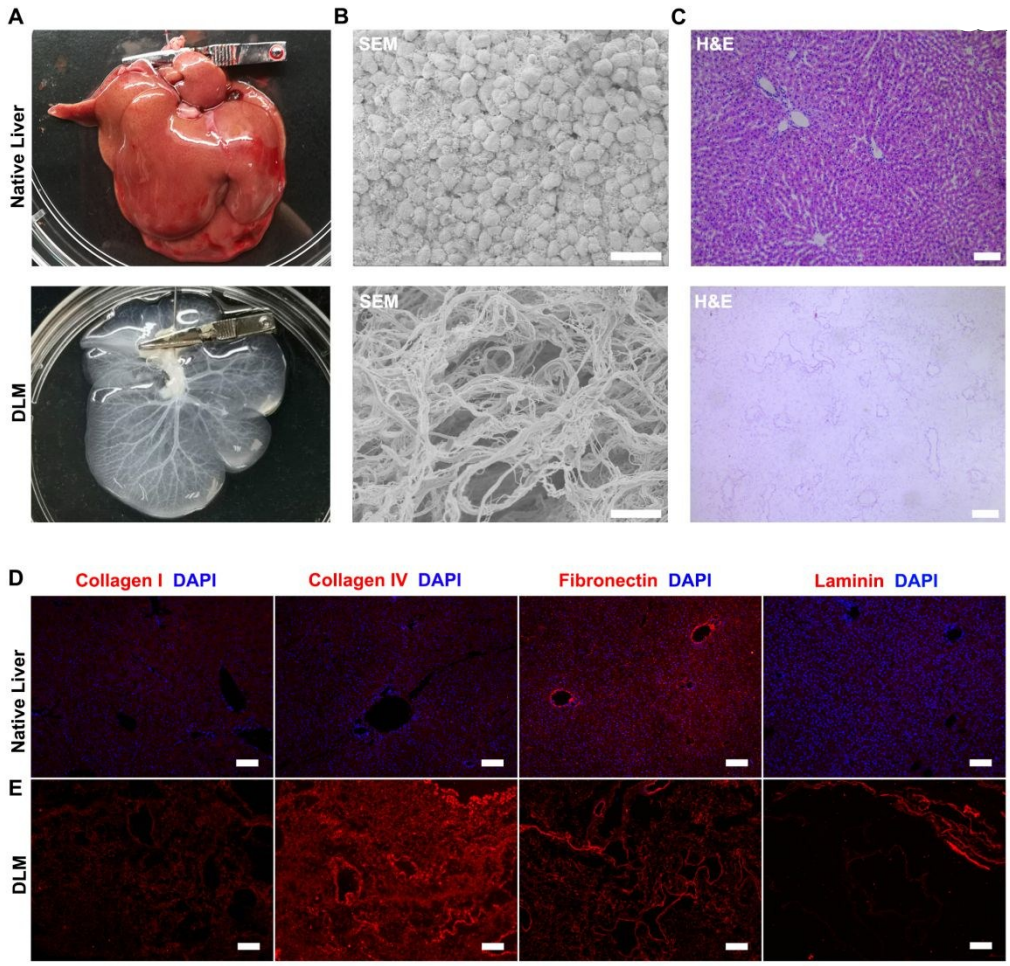

Figure 2. Characterization of the native liver matrix and DLM. (A) Native rat liver compared to the white/transparent DLM. (B) SEM characterization of the native liver compared to the acellular liver scaffold. Scale bar: 100 μm. Fine reticular matrix fibers were observed in DLM. (C) H&E staining for comparison of natural and acellular livers. (D-E) Collagen I, collagen IV, fibronectin, and laminin from both the native liver and DLM were all immuno-stained in red. Sections were counterstained with DAPI (blue). Scale bar: 100 μm (A, C, D, E) and 50 μm (B).

Fabrication of the bioengineered whole liver

Approximately 2 × 10^7 HepG2 cells were seeded into the DLM. The recellularized livers were transferred to a perfusion-based oxygenated bioreactor for culturing *in vitro*. Bioengineered whole livers were cultured for 14 days with continuous perfusion of oxygenated media and observed on days 1, 3, 7, and 14 (Figure 3A-B). HepG2 cells seeded in decellularized liver scaffolds grew into 3D nodules. In daily visual inspections, both the size and density of the nodules formed by mixing the cells with

5% GelMA throughout the culturing period was greater than the nodules formed *via* direct seeding in the naked DLM (Figure 3A-B). After culturing in identical 3D environments, the DLM/GelMA displayed cell viability values of 97.74 ± 3.63%, 97.14 ± 1.60%, 94.55 ± 3.42%, and 98.02 ± 1.57% on days 1, 3, 7, and 14, respectively. Comparatively, the direct seeding model displayed cell viability values of 96.39 ± 2.63%, 97.40 ± 0.54%, 89.49 ± 3.83%, and 95.51 ± 2.48% on days 1, 3, 7, and 14, respectively, showing no significant difference ($p > 0.05$) (Figure 3C-E). However, the DLM/GelMA model displayed cell growth rates of 71.15 ± 2.06%, 87.23 ± 19.97%, 89.74 ± 19.01%, and 93.95 ± 37.39% on days 1, 3, 7, and 14, respectively. On the other hand, the direct seeding model displayed values of 41.93 ± 11.94%, 47.16 ± 77.62%, 64.31 ± 31.80%, and 83.05 ± 57.26%, respectively. These results demonstrated that the cell growth rate was significantly higher in the DLM/GelMA than the direct seeding model ($p < 0.05$) (Figure 3 F).

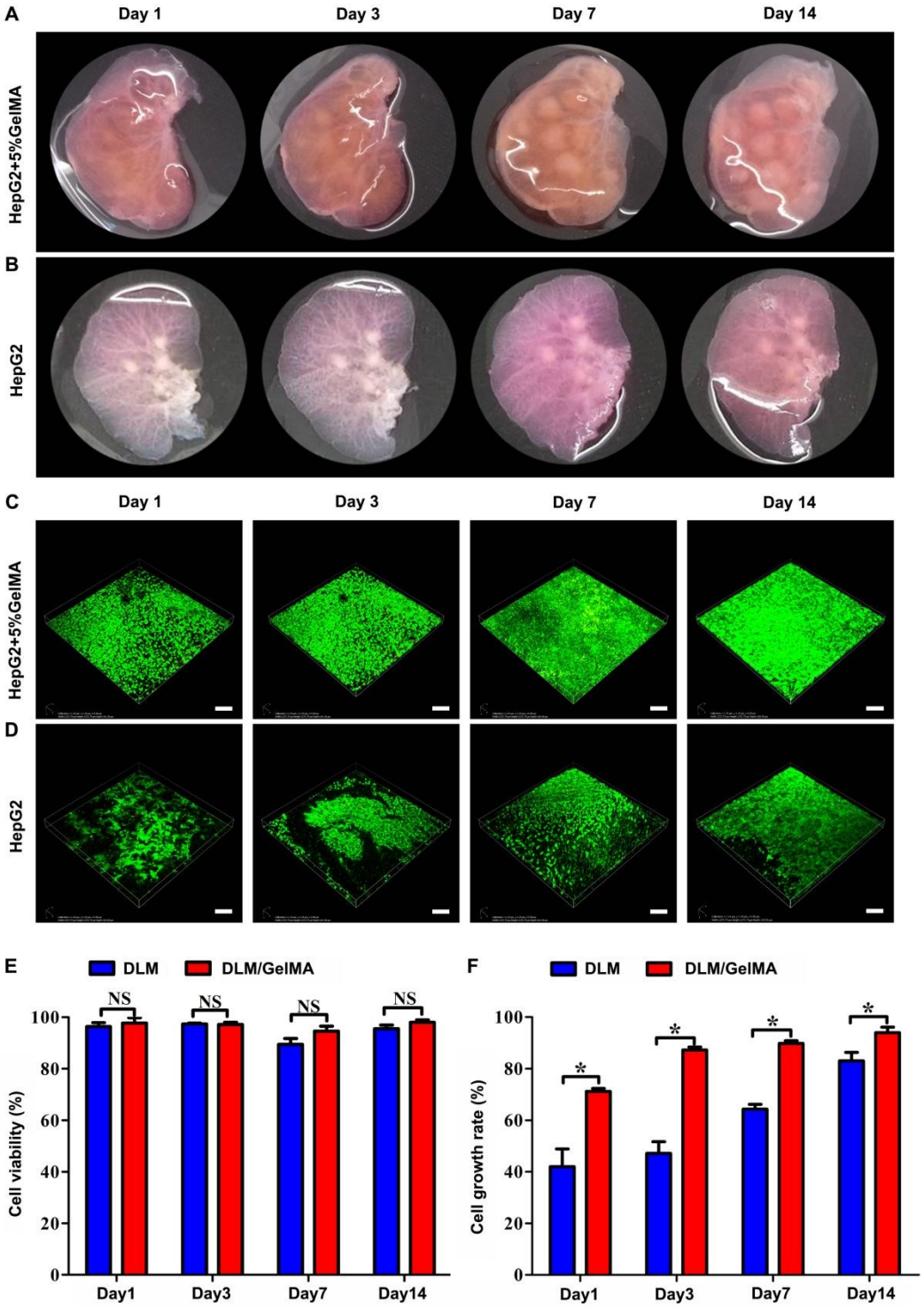

Figure 3. Biofabrication and characterization of the DLM/GelMA-based bioengineered whole liver. The DLM/GelMA-based bioengineered whole liver was fabricated by incorporating approximately 2×10^7 HepG2 cells with DLM/GelMA. The resultant DLM/GelMA-based bioengineered whole liver was then cultured in a bioreactor with 95% of oxygen for 14 days. As a control, GelMA was not incorporated into the bioengineered whole liver. The gross images of the

DLM/GelMA-based bioengineered whole liver (A) and the control within the naked DLM (B) were observed on Days 1, 3, 7, and 14. The Live/Dead staining of the DLM/GelMA-based bioengineered whole liver (C) and the control within the naked DLM (D) were observed on Days 1, 3, 7, and 14. The fluorescence images were taken from a representative region with a depth of approximately 100 μm in two bioengineered whole livers. Scale bar: 100 μm. Based on the representative images shown in (C) and (D), the cell viability of HepG2 cells (E) and the cell growth rate (F) were analyzed and compared between these two bioengineered whole livers. Data are averaged from 3 samples and presented as Avg ± SD (* indicates that p is less than 0.05, and NS indicates that p is more than 0.05).

Oxygen delivery to the bioengineered whole liver within the bioreactor

By establishing the model, the concentration of oxygen in the surface layer of the DLM/GelMA whole liver was 0.19 mol m^{-3}, and the concentration of oxygen delivery to the center of the whole liver was 0.04 mol m^{-3} (Figure 4A). Hypoxia staining showed less hypoxic hepatocytes in the surface and center of the bioengineered whole liver (Figure 4B). Live/Dead staining showed a cell viability of more than 90% in the surface and center of the novel bioengineered whole liver (Figure 4C-D).

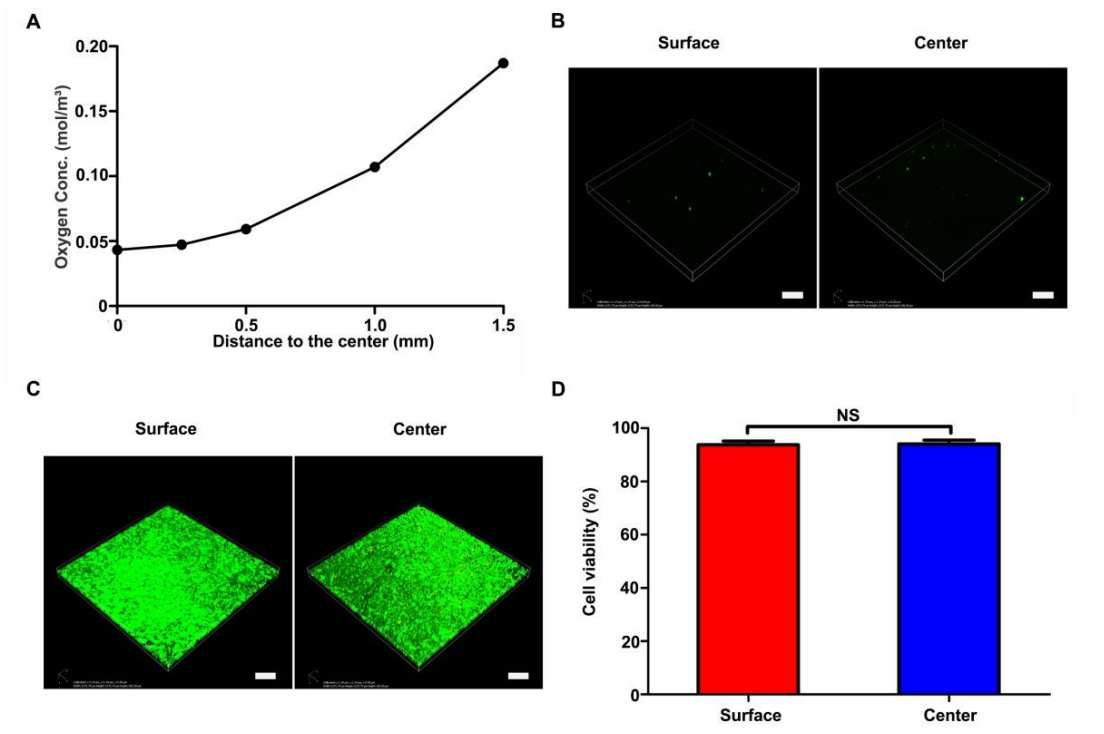

Figure 4. Oxygen delivery to the bioengineered whole liver *via* a bioreactor. (A) Calculation of oxygen concentration in the DLM/GelMA-based bioengineered whole

liver in a perfusion-based oxygenated bioreactor. (B) After 14 days of culture the surface and center cells of DLM/GelMA-based bioengineered whole liver were stained with a hypoxia kit (B) or Live/Dead assay (C). Hypoxic cells were stained green in (B), while living cells were stained green and dead cells were stained red in (C). (D) Based on the representative images shown in (C), the cell viability of HepG2 cells was analyzed.

Functional characterization of the bioengineered whole liver

The synthesis and transformation functions of HepG2 cells mixed in 5% GelMA and then injected in DLM were compared to that of HepG2 cells directly injected into the naked DLM. To this end, the albumin levels secreted by HepG2 cells in both models over 14 days were compared (Figure 5A). The amount of ALB secreted on days 1, 3, 7, and 14 by cells mixed with GelMA was 13.54 ± 0.19, 14.18 ± 0.52, 13.93 ± 0.84, and 12.76 ± 0.17 μg mL^{-1}, respectively. These values were significantly higher than that of HepG2 cells directly seeded in naked DLM on days 1, 3, 7, and 14 with values of 11.37 ± 0.53, 12.52 ± 0.20, 12.05 ± 0.27, and 10.99 ± 0.53 μg mL^{-1}, respectively ($p < 0.05$) (Figure 5A). Similarly, when HepG2 cells were mixed with 5% GelMA in DLM, the amounts of urea produced on days 1, 3, 7, and 14 were 1.34 ± 0.12, 1.28 ± 0.09, 1.30 ± 0.09, and 1.69 ± 0.08 mmol L^{-1}, respectively. In contrast, the amounts of urea produced by HepG2 cells directly seeded in naked DLM were 0.95 ± 0.08, 1.06 ± 0.01, 1.05 ± 0.07, and 1.40 ± 0.11 mmol L^{-1}, respectively. These results indicated that under perfusion-based oxygenation culturing conditions, HepG2 cells in DLM/GelMA-based bioengineered whole liver maintained significantly higher levels of urea production than in the naked DLM ($p < 0.05$, Figure 5B).

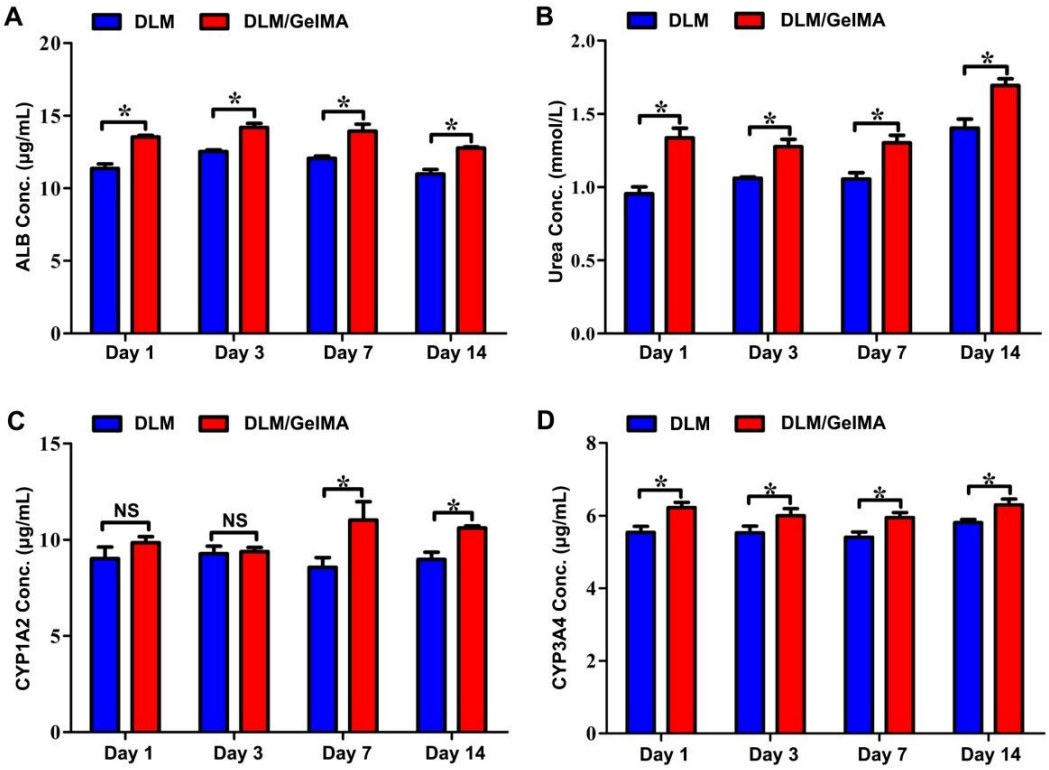

Figure 5. Functional characterization of HepG2 cells in the bioengineered whole liver. Production of albumin (A) and urea (B) in the DLM/GelMA-based bioengineered whole liver compared to those in the naked DLM. The main metabolic enzyme expression levels of HepG2 cells CYP1A2 (C) and CYP3A4 (D) in the DLM/GelMA compared to those in the naked DLM. Data are averaged from 3 samples and presented as Avg ± SD (* indicates that p is less than 0.05, and NS indicates that p is more than 0.05).

The expression levels of key enzymes in liver drug metabolism, specifically CYP1A2 and CYP3A4 in HepG2 cells, were investigated. The amount of CYP1A2 expressed on days 1, 3, 7, and 14 by cells mixed with DLM/GelMA was 9.85 ± 0.32, 9.38 ± 0.22, 11.03 ± 0.95, and 10.61 ± 0.10 ng mL^{-1}, respectively. Comparatively, the amount of CYP1A2 expressed on days 1, 3, 7, and 14 by cells directly seeded in the naked DLM was 9.02 ± 0.60, 9.27 ± 0.39, 8.57 ± 0.51, and 8.97 ± 0.38 ng mL^{-1}, respectively. Therefore, the CYP1A2 expressed was not significantly different on days 1 and 3. However, the amount of CYP1A2 expressed by cells mixed with GelMA was significantly higher on days 7 and 14 than that of cells directly seeded in the naked DLM ($p < 0.05$, Figure 5C). In contrast, the amount of CYP3A4 expressed

on days 1, 3, 7, and 14 by cells mixed with GelMA was 6.22 ± 0.15, 6.00 ± 0.19, 5.95 ± 0.14, and 6.30 ± 0.16 ng mL^{-1}, respectively. Comparatively, the amount of CYP3A4 expressed on days 1, 3, 7, and 14 by cells directly seeded in the naked DLM was 5.54 ± 0.17, 5.53 ± 0.18, 5.41 ± 0.15, and 5.81 ± 0.09 ng mL^{-1}, respectively. Thus, the expression of CYP3A4 in HepG2 cells seeded in the DLM/GelMA was significantly higher than that of cells directly seeded in the naked DLM in every observable time frame ($p < 0.05$, Figure 5D).

Ammonia reduction by the bioengineered whole liver

To observe the detoxification function of the bioengineered whole liver, various concentrations of NH_4Cl were added to the culture solution. Cell viability, ammonia concentrations, and urea concentrations were assessed accordingly. Cell viability was found to be 96.09 ± 2.29%, 90.30 ± 2.31%, 83.02 ± 6.97%, 53.94 ± 2.59%, and 42.79 ± 4.21% at concentrations of 5, 10, 30, 60, and 120 mM NH_4Cl, respectively (Figure 6A). The results illustrated a negative correlation between NH_4Cl concentration and cell viability. By adding 10 mM NH_4Cl to the culture medium within 48 h, the ammonia concentrations in the DLM/GelMA were found to decrease from 5.66 ± 1.24 mmol L^{-1} to 3.11 ± 0.65 mmol L^{-1}, a significant reduction of approximately 45% ($p < 0.05$). Cells in the direct seeding model showed an insignificant decrease in ammonia concentration from 5.66 ± 1.24 mmol L^{-1} to 4.24 ± 1.27 mmol L^{-1} ($p > 0.05$) (Figure 6C). After 48 hours, urea production by HepG2 cells in the DLM/GelMA increased from the initial 346.49 ± 4.97 μmol L^{-1} to 556.78 ± 57.20 μmol L^{-1}, whereas urea production by HepG2 cells in the direct seeding model was found to increase from 321.49 ± 42.24 μmol L^{-1} to 443.82 ± 0.50 μmol L^{-1}. The results showed that the amount of urea produced by HepG2 cells increased significantly with the addition of NH_4Cl solution ($p < 0.05$) (Figure 6D). Therefore, the results indicated that HepG2 cells in the DLM/GelMA had a better ammonia detoxification function than that of HepG2 cells directly seeded in the naked DLM.

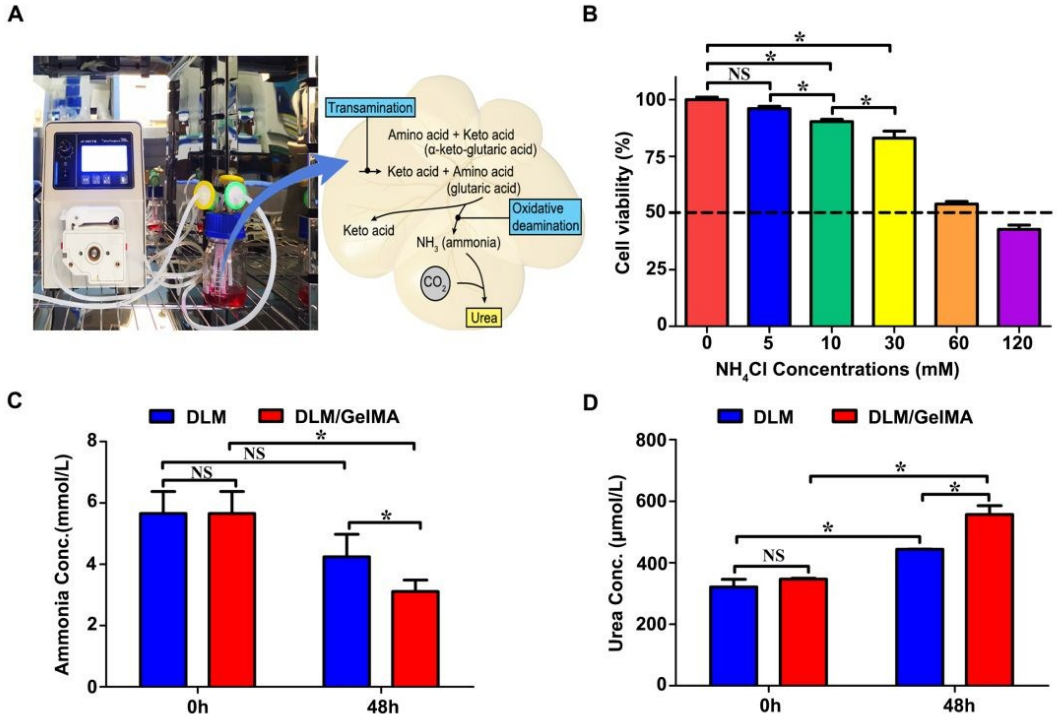

Figure 6. Detoxification of high levels of ammonia *via* the DLM/GelMA-based bioengineered whole liver. (A) The DLM/GelMA-based bioengineered whole liver was cultured in a bioreactor with a continuous flow of DMEM at a perfusion rate of 3 mL min^{-1}) and 95% of oxygen. The mechanism of biotransformation of ammonia to urea was leveraged for ammonia reduction. (B) The viability of HepG2 cells was evaluated following incubation with 5, 10, 30, 60, and 120 mM of NH_4Cl for 24 hours. (C) The concentration of NH_4Cl was measured at 48 h after adding 10 mM of NH_4Cl to the DLM/GelMA-based whole liver and HepG2 cells seeded into the naked DLM. (D) The concentration of urea was also measured after the NH_4Cl (10 mM) treatment for 48 hours in both models. Data are averaged from 3 samples and presented as Avg ± SD (* indicates that p is less than 0.05, and NS indicates that p is more than 0.05).

Discussion

BLSS is a promising strategy for the clinical management of liver failure and HE, especially in the absence of readily available liver transplantation. In this study, we developed a novel BLSS integrated with a GelMA/DLM-based bioengineered whole liver, aiming at preventing HE in liver failure patients (Figure 1). Of note, the addition of GelMA in the bioengineered whole liver not only improved the adhesion and

proliferation of hepatocytes, but also provided biomechanical support to maintain the space configuration of native liver tissues, addressing a persisting challenge for the fabrication of bioengineered whole liver. In addition, the combination of GelMA with DLM provides biological factors (collagens and growth factors), 3D scaffolds, and biomechanical cues, offering a biomimetic ECM for hepatocytes in the bioengineered whole liver. Due to the mimicry of the ECM in which hepatocytes reside *in vivo*, hepatocytes exhibited a cell viability of more than 90% over the course of 14 days and showed elevated production of albumin and CYP enzymes. More importantly, the bioengineered whole liver significantly reduced ammonia by 45%, whereas the hepatocytes seeded into the naked DLM showed no significant reduction. Thus, this novel BLSS with the GelMA/DLM-based bioengineered whole liver showed great potential to support liver failure patients and to help minimize the progression to HE.

The ECM plays a vital role in controlling cell proliferation, metabolism, and function as well as cell-to-cell interactions[28-30]. In this study, we mimicked the ECM of hepatocytes *in vivo* in terms of biological composition, biomechanical support, and 3D liver-specific space configuration. Previously, DLM has been utilized as the scaffolds for fabrication of bioengineered livers, because collagens, growth factors and vascular structures are preserved and partially biologically active, serving as a good basis for liver tissue regeneration[20, 22, 27]. Owing to this advantage, we utilized DLM scaffolds for seeding hepatocytes to fabricate a bioengineered whole liver. However, the adhesion of hepatocytes within DLM, particularly in the presence of continuous flow of culture media, remained challenging. To overcome this challenge, we introduced 5% GelMA to provide mechanical support so as to promote cell adhesion and immobilization within DLM. GelMA, in contrast to naturally derived ECM components such as gelatin, collagen, or hyaluronic acid which suffer from inconsistency between batch production[31, 32], can be made to reduce lot-to-lot variation and to improve reproducibility. More importantly, 5% GelMA, once solidified within DLM, provides biologically relevant stiffness and biomechanical properties resembled to native liver ECM *in vivo*[33, 34]. Studies have shown that the stiffness in ECM can promote stem cell differentiation[35], maintain cell functionality[36], and reverse aged oligodendrocyte progenitor cells[37]. With this physiologically relevant stiffness and mechanical support, hepatocytes can be well immobilized within DLM with good cell viability (more than 90%), cell engraftment and cell

growth (Figure 3E-F). In addition, GelMA helped maintain the space configuration of native liver tissues in the bioengineered whole liver (Figure 3A). In contrast, the bioengineered whole liver using the naked DLM only tended to collapse due to the absence of mechanical support (Figure 3B). Thus, the DLM/GelMA-based bioengineered whole liver established a biomimetic ECM for hepatocytes to reside and grow in a close-to-native manner.

Although the liver-specific ECM has been mimicked to a great extent, vascular structures and blood flow are missing in the DLM/GelMA-based bioengineered whole liver. Therefore, oxygen supply might become an issue, since (1) the liver coordinates high metabolic functions and typically consumes 20% to 33% of total oxygen *in vivo*[38]; (2) under hypoxic conditions, hepatocytes exhibits pathological, morphological changes and lose critical biological functions as demonstrated in a bioreactor[39]; and (3) the 21% oxygen content of the atmosphere does not provide sufficient oxygen for bioengineered livers with high cell densities to survive[40]. To meet the high demand for oxygen in bioengineered liver, we cultured it in a bioreactor with a continuous flow of culture media (3 mL min^{-1}) and 95% of oxygen. According to the modeling of oxygen diffusion, the oxygen level at the surface and center of the bioengineered liver was 0.19 mol m^{-3} and 0.04 mol m^{-3}, respectively (Figure 4A), indicating that there was no oxygen deprivation within the entire bioengineered liver. Indeed, there was no hypoxia in neither the surface nor the center of the bioengineered whole liver (Figure 4B). Meanwhile, the viability in both the surface and the center of the bioengineered whole liver showed no significant difference (Figure 4D), indicating that the oxygen supply was sufficient within the biofabricated liver. Taken together, a high level of oxygen (95%) within the bioreactor can provide sufficient oxygen *via* diffusion and compensate for the lack of media flow within the DLM/GelMA based bioengineered whole liver.

Hepatocytes grown in liver-specific ECM with sufficient oxygen supply showed enhanced biosynthetic and biotransformation capabilities, which lays the foundation for the development of the novel BLSS. First, HepG2 cells within the DLM/GelMA-based bioengineered liver showed elevated secretion of albumin (Figure 5A), which is essential for expanding plasma volume, performing antioxidant activity, and regulating the immune systems [41]. Second, the DLM/GelMA-based

bioengineered whole liver showed significantly higher levels of CYP3A4 and CYP1A2, which are key members of the cytochrome P450 (CYP) family for liver metabolism[42, 43], compared to the bioengineered liver with the naked DLM (Figure 5C-D). In addition to enhanced biosynthetic capabilities, the DLM/GelMA-based bioengineered whole liver was able to convert high concentrations of ammonia to urea, which is essential to avert the progression of HE in liver failure patients. In the presence of 10 mM of NHCl[44], the DLM/GelMA-based bioengineered whole liver successfully reduced ammonia from 5.66 mmol L^{-1} to 3.11 mmol L^{-1}, whereas, the whole liver direct seeding of hepatocytes in the naked DLM showed no significant reduction. The reason why the DLM group did not show significant effects on ammonia conversion was probably due to low cell engraftment and cell growth in the absence of biomechanical support provided by GelMA. The capability of ammonia reduction can be further improved by using HepG2 cells that are gene-edited to stably overexpress human arginase and human ornithine transcarbamylase[45, 46]. Thus, the enhanced biosynthetic and biotransforming capabilities of the DLM/GelMA-based bioengineered whole liver potentially enable the development of BLSS to support liver failure patients and prevent the occurrence of HE.

Although this proof-of-concept study has shown increased functionality of BLSS with integration of DLM/GelMA based bioengineered whole liver, it would further enhance the scientific merit and improve clinical utility from the following aspects. First, it is better to compare our DLM/GelMA-based bioengineered whole liver with other BLSS to verify the functionality of DLM/GelMA in BLSS. Currently, advances in BLSS have been attributed to the development of hollow fiber cartridges[47], the formation of hepatocyte spheroids under oscillating culture conditions[48], the integration of biomaterials such as alginate to form hepatocyte aggregates[49, 50], and the development of human functional hepatocytes (*i.e.,* hiHeps) by lineage conversion[51]. Different from these efforts, our BLSS is characterized by the integration of DLM/GelMA based bioengineered whole liver, and this new research direction needs further validation with respect to cell viability and functionality. Second, it would provide more insights to confirm the enhanced functionality of the BLSS by normalizing the number of live hepatocytes within DLM. Given the technical difficulty, the current study can only attribute the enhanced functionality of the BLSS to the increase in the number of live hepatocytes within the bioengineered

whole liver, or to the enhancement of hepatocyte functionalities, or both. Third further validation is needed to confirm the safety and clinical utility of integrating DLM/GelMA based bioengineered whole liver in BLSS to support liver failure patients and to prevent HE in pre-clinical and clinical studies.

Conclusion

In this study, we developed a novel BLSS integrated with a DLM/GelMA-based bioengineered whole liver. Owing to the provision of a liver-specific ECM and sufficient oxygen supply, the fabricated whole liver demonstrated enhanced secretion of albumin, production of CYP enzymes, and conversion of ammonia to urea, which shows great potential to support liver failure patients *in vitro* and minimize the chances of developing HE. Nevertheless, further validation is needed to confirm the ability of the bioengineered whole liver and bioreactor to support liver failure in animal research and clinical trials.

Conflicts of interest

The authors confirm that there are no known conflicts of interest associated with this publication and there has been no significant financial support for this work that could have influenced its outcome.

Acknowledgments

We acknowledge the National Key Research and Development Program (2016YFC1101302) from Ministry of Science and Technology of China, General Program (31871016) from the National Natural Science Foundation of China, National Key Scientific Instrument and Equipment Development Projects (61827806), the supports from National Major Science and Technology Projects (2018ZX10732401-003-007), Key Research and Development Program (2019C03029) from the Science and Technology Department of Zhejiang Province, start-up fund (1-ZE7S), central research fund (G-YBWS) and intra-faculty fund (1-ZVPC) from the Hong Kong Polytechnic University.

References

1. S. K. Asrani, H. Devarbhavi, J. Eaton and P. S. Kamath, *J Hepatol*, 2019, **70**, 151-171.
2. E. F. Wijdicks, *N Engl J Med*, 2016, **375**, 1660-1670.
3. C.-W. Lee, Y.-F. Chen, H.-H. Wu and O. K. Lee, *Gastroenterology*, 2018, **154**, 46-56.
4. W. Bernal, R. Jalan, A. Quaglia, K. Simpson, J. Wendon and A. Burroughs, *The Lancet*, 2015, **386**, 1576-1587.
5. A. Kribben, G. Gerken, S. Haag, S. Herget-Rosenthal, U. Treichel, C. Betz, C. Sarrazin, E. Hoste, H. Van Vlierberghe, A. Escorsell, C. Hafer, O. Schreiner, P. R. Galle, E. Mancini, P. Caraceni, C. J. Karvellas, H. Salmhofer, M. Knotek, P. Gines, J. Kozik-Jaromin, K. Rifai and H. S. Group, *Gastroenterology*, 2012, **142**, 782-789 e783.
6. B. Carpentier, A. Gautier and C. Legallais, *Gut*, 2009, **58**, 1690-1702.
7. F. Meng, A. Assiri, D. Dhar and D. Broering, *Liver Int*, 2017, **37**, 1759-1772.
8. Y. Li, Q. Wu, Y. Wang, C. Weng, Y. He, M. Gao, G. Yang, L. Li, F. Chen, Y. Shi, B. P. Amiot, S. L. Nyberg, J. Bao and H. Bu, *Theranostics*, 2018, **8**, 5562-5574.
9. A. Damania, A. Kumar, A. K. Teotia, H. Kimura, M. Kamihira, H. Ijima, S. K. Sarin and A. Kumar, *ACS Appl Mater Interfaces*, 2018, **10**, 114-126.
10. J. L. Lise L. Kjaergard, Bodil Als-Nielsen,Christian Gluud, *The Journal of American Medical Association*, 2003, **289**, 217-222.
11. J. Wang, F. Chen, L. Liu, C. Qi, B. Wang, X. Yan, C. Huang, W. Hou, M. Q. Zhang, Y. Chen and Y. Du, *Biomaterials*, 2016, **91**, 11-22.
12. Y. Wang, X. Yu, E. Chen and L. Li, *Stem Cell Res Ther*, 2016, **7**, 71.
13. J. Kasuya, R. Sudo, R. Tamogami, G. Masuda, T. Mitaka, M. Ikeda and K. Tanishita, *Biomaterials*, 2012, **33**, 2693-2700.
14. J. Zhang, X. Zhao, L. Liang, J. Li, U. Demirci and S. Wang, *Biomaterials*, 2018, **157**, 161-176.
15. H. Qi, M. Ghodousi, Y. Du, C. Grun, H. Bae, P. Yin and A. Khademhosseini, *Nature Communications*, 2013, **4**.
16. J. G. Torres-Rendon, T. Femmer, L. De Laporte, T. Tigges, K. Rahimi, F. Gremse, S. Zafarnia, W. Lederle, S. Ifuku, M. Wessling, J. G. Hardy and A. Walther, *Adv Mater*, 2015, **27**, 2989-2995.
17. L. B. Chen S, Carlson M A, Gombart A F, Reilly D A and Xie J, *Nanomedicine*, 2017, **12**, 1335-1352.
18. L. Cheng, X. Sun, X. Zhao, L. Wang, J. Yu, G. Pan, B. Li, H. Yang, Y. Zhang and W. Cui, *Biomaterials*, 2016, **83**, 169-181.
19. J. S. Lee, J. Shin, H. M. Park, Y. G. Kim, B. G. Kim, J. W. Oh and S. W. Cho, *Biomacromolecules*, 2014, **15**, 206-218.
20. S. Lu, F. Cuzzucoli, J. Jiang, L. G. Liang, Y. Wang, M. Kong, X. Zhao, W. Cui, J. Li and S. Wang, *Lab Chip*, 2018, **18**, 3379-3392.
21. R. Ji, N. Zhang, N. You, Q. Li, W. Liu, N. Jiang, J. Liu, H. Zhang, D. Wang, K. Tao and K. Dou, *Biomaterials*, 2012, **33**, 8995-9008.
22. K. M. Park, K. H. Hussein, S. H. Hong, C. Ahn, S. R. Yang, S. M. Park, O. K. Kweon, B. M. Kim and H. M. Woo, *Tissue Eng Part A*, 2016, **22**, 449-460.
23. G. Mazza, K. Rombouts, A. Rennie Hall, L. Urbani, T. Vinh Luong, W. Al-Akkad, L. Longato, D. Brown, P. Maghsoudlou, A. P. Dhillon, B. Fuller, B. Davidson, K. Moore, D. Dhar, P. De Coppi, M. Malago and M. Pinzani, *Sci*

Rep, 2015, **5**, 13079.
24. A. J. Davidson, M. J. Ellis and J. B. Chaudhuri, *Biotechnol Bioeng*, 2010, **106**, 980-988.
25. J. F. P. II, *Artificial Organs*, 2004, **28**, 83-98.
26. F. T. Lee-Montiel, S. M. George, A. H. Gough, A. D. Sharma, J. Wu, R. DeBiasio, L. A. Vernetti and D. L. Taylor, *Exp Biol Med (Maywood)*, 2017, **242**, 1617-1632.
27. Y. Wang, D. Wu, G. Wu, J. Wu, S. Lu, J. Lo, Y. He, C. Zhao, X. Zhao, H. Zhang and S. Wang, *Theranostics*, 2020, **10**, 300-311.
28. B. S. Kim, H. Kim, G. Gao, J. Jang and D. W. Cho, *Biofabrication*, 2017, **9**, 034104.
29. K. J. Jin Y, Lee JS, Min s, Kim s, Ahn DH, Kim YG, Cho SW., *Adv. Funct. Mater.*, 2018, **28**, 1801954.
30. P. M. Baptista, M. M. Siddiqui, G. Lozier, S. R. Rodriguez, A. Atala and S. Soker, *Hepatology*, 2011, **53**, 604-617.
31. D. W. Hutmacher, D. Loessner, S. Rizzi, D. L. Kaplan, D. J. Mooney and J. A. Clements, *Trends in Biotechnology*, 2010, **28**, 125-133.
32. D. W. Hutmacher, *Nat Mater*, 2010, **9**, 90-93.
33. E. Kaemmerer, F. P. W. Melchels, B. M. Holzapfel, T. Meckel, D. W. Hutmacher and D. Loessner, *Acta Biomaterialia*, 2014, **10**, 2551-2562.
34. T. Xia, R. Zhao, W. Liu, Q. Huang, P. Chen, Y. N. Waju, M. K. Al-Ani, Y. Lv and L. Yang, *J Cell Physiol*, 2018, **233**, 6996-7006.
35. Y. Ma, M. Lin, G. Huang, Y. Li, S. Wang, G. Bai, T. J. Lu and F. Xu, *Adv Mater*, 2018, **30**, e1705911.
36. J. Sarkar, S. C. Kamble, R. Patil, A. Kumar and S. W. Gosavi, *Biotechnol Bioeng*, 2020, **117**, 567-579.
37. M. Segel, B. Neumann, M. F. E. Hill, I. P. Weber, C. Viscomi, C. Zhao, A. Young, C. C. Agley, A. J. Thompson, G. A. Gonzalez, A. Sharma, S. Holmqvist, D. H. Rowitch, K. Franze, R. J. M. Franklin and K. J. Chalut, *Nature*, 2019, **573**, 130-134.
38. T. M. Rotem A, Tompkins RG, Yarmush ML., *Biotechnol Bioeng* 1992, **40**, 1286-1291.
39. K. Montagne, H. Huang, K. Ohara, K. Matsumoto, A. Mizuno, K. Ohta and Y. Sakai, *J Biosci Bioeng*, 2011, **112**, 485-490.
40. Y. Nosé, *Artificial Organs*, 2004, **28**, 807-812.
41. L. Cagnon and O. Braissant, *Brain Res Rev*, 2007, **56**, 183-197.
42. H. Lee, S. Chae, J. Y. Kim, W. Han, J. Kim, Y. Choi and D. W. Cho, *Biofabrication*, 2019, **11**, 025001.
43. M. Yamada, R. Utoh, K. Ohashi, K. Tatsumi, M. Yamato, T. Okano and M. Seki, *Biomaterials*, 2012, **33**, 8304-8315.
44. V. Rangroo Thrane, A. S. Thrane, F. Wang, M. L. Cotrina, N. A. Smith, M. Chen, Q. Xu, N. Kang, T. Fujita, E. A. Nagelhus and M. Nedergaard, *Nat Med*, 2013, **19**, 1643-1648.
45. N. Tang, Y. Wang, X. Wang, L. Zhou, F. Zhang, X. Li and Y. Chen, *J Cell Biochem*, 2012, **113**, 518-527.
46. Y. Wang, L. Chang, J. Zhai, Q. Wu, D. Wang and Y. Wang, *J Cell Mol Med*, 2017, **21**, 3214-3223.
47. C. Legallais, D. Kim, S. M. Mihaila, M. Mihajlovic, M. Figliuzzi, B. Bonandrini, S. Salerno, F. A. Yousef Yengej, M. B. Rookmaaker, N. Sanchez Romero, P. Sainz-Arnal, U. Pereira, M. Pasqua, K. G. F. Gerritsen, M. C.

Verhaar, A. Remuzzi, P. M. Baptista, L. De Bartolo, R. Masereeuw and D Stamatialis, *Adv Healthc Mater*, 2018, **7**, e1800430.
48. J. M. Glorioso, S. A. Mao, B. Rodysill, T. Mounajjed, W. K. Kremers, F. Elgilani, R. D. Hickey, H. Haugaa, C. F. Rose, B. Amiot and S. L. Nyberg, *J Hepatol*, 2015, **63**, 388-398.
49. H. F. Chan, Y. Zhang and K. W. Leong, *Small*, 2016, **12**, 2720-2730.
50. M. Desille, S. Mahler, P. Seguin, Y. Malledant, B. Fremond, V. Sebille, A. Bouix, J. F. Desjardins, A. Joly, J. Desbois, Y. Lebreton, J. P. Campion and B. Clement, *Crit Care Med*, 2002, **30**, 658-663.
51. X. L. Shi, Y. Gao, Y. Yan, H. Ma, L. Sun, P. Huang, X. Ni, L. Zhang, X. Zhao, H. Ren, D. Hu, Y. Zhou, F. Tian, Y. Ji, X. Cheng, G. Pan, Y. T. Ding and L. Hui, *Cell Res*, 2016, **26**, 206-216.